ADVANCED MATERIALS
www.advmat.de

Rapid Identification of DNA Fragments through Direct Sequencing with Electro-Optical Zero-Mode Waveguides

*Fatemeh Farhangdoust, Feng Cheng, Wentao Liang, Yongmin Liu, and Meni Wanunu**

In contrast to sequence-specific techniques such as polymerase chain reaction, DNA sequencing does not require prior knowledge of the sample for surveying DNA. However, current sequencing technologies demand high inputs for a suitable library preparation, which typically necessitates DNA amplification, even for single-molecule sequencing methods. Here, electro-optical zero-mode waveguides (eZMWs) are presented, which can load DNA into the confinement of zero-mode waveguides with high efficiency and negligible DNA fragment length bias. Using eZMWs, highly efficient voltage-induced loading of DNA fragments of various sizes from ultralow inputs (nanogram-to-picogram levels) is observed. Rapid DNA fragment identification is demonstrated by burst sequencing of short and long DNA molecules (260 and 20 000 bp) loaded from an equimolar picomolar-level concentration mixture in just a few minutes. The device allows further studies in which low-input DNA capture is essential, for example, in epigenetics, where native DNA is required for obtaining modified base information.

1. Introduction

Rapid Identification of DNA molecules in an unknown sample could have breakthrough impacts on the diagnosis of infectious diseases, mutation, and discovery of pathogens. While sequence-specific techniques such as polymerase chain reaction (PCR)[1] and other amplification methods identify a host of species through a sequence-guided search, DNA sequencing is required for surveying DNA in a sample when no prior knowledge of the sample is available. Both second-generation and third-generation (i.e., single-molecule) sequencing methods can be applied for DNA surveying; however, both require sufficient input material for library preparation which typically requires some DNA amplification steps,[2] despite third-generation sequencing being able to perform direct sequencing on native molecules when ample amounts can be made available.[3]

In single-molecule, real-time (SMRT) sequencing, individual nucleotides are monitored in real time during DNA strand replication by an individual DNA polymerase tracking the incorporation of multicolor fluorescently labeled nucleotides.[3a] The DNA template to be sequenced is loaded to the bottom of 100 nm diameter nanowells called zero-mode waveguides (ZMWs) via a diffusion process, which naturally favors the capture of shorter DNA molecules due to the size constraints of the wells.[3b,4] To obtain reads from long fragments, size-selection systems are used, in which short fragments are removed through gel electrophoresis.[5] Overall, high input DNA amounts (>3 µg per 1 Gb genome) are required in SMRT sequencing protocols,[5,6] and although library preparation methods from sub-nanogram DNA are available,[7] a DNA loading limitation from such low input amounts prevents efficient readout from low inputs.

The need for new platforms to efficiently load DNA fragments of various sizes into ZMWs with no length bias and from ultralow inputs (picogram levels) has led to the development of several types of electrically actuatable ZMWs including nanopore ZMWs (NZMWs)[8] and porous ZMWs (PZMWs).[9] In these devices, voltage application across the devices leads to ion flow across the porous base of the ZMWs, which leads to electrokinetics-mediated loading of biomolecules (DNA, RNA, and proteins). In contrast to diffusion-based loading, electrokinetics-mediated loading features low size bias and sub-nanogram DNA input requirements. However, these devices all rely on a freestanding ultrathin membrane, which somewhat compromises the device longevity and increases the background photoluminescence. To overcome these issues, we have developed here electro-optical ZMWs (eZMWs), a novel design of electrically actuatable ZMWs in which no freestanding membranes are required. In this device, waveguides have embedded electrodes at their bases that allow voltage-induced capture of DNA molecules into the eZMWs. Our new device features scalable architecture, enhanced device stability as compared

F. Farhangdoust, M. Wanunu
Department of Bioengineering
Northeastern University
Boston, MA 02115, USA
E-mail: wanunu@neu.edu
F. Cheng, Y. Liu
Department of Electrical and Computer Engineering
Northeastern University
Boston, MA 02115, USA
W. Liang, M. Wanunu
Department of Physics
Northeastern University
Boston, MA 02115, USA
M. Wanunu
Department of Chemistry and Chemical Biology
Northeastern University
Boston, MA 02115, USA
The ORCID identification number(s) for the author(s) of this article can be found under https://doi.org/10.1002/adma.202108479.

DOI: 10.1002/adma.202108479

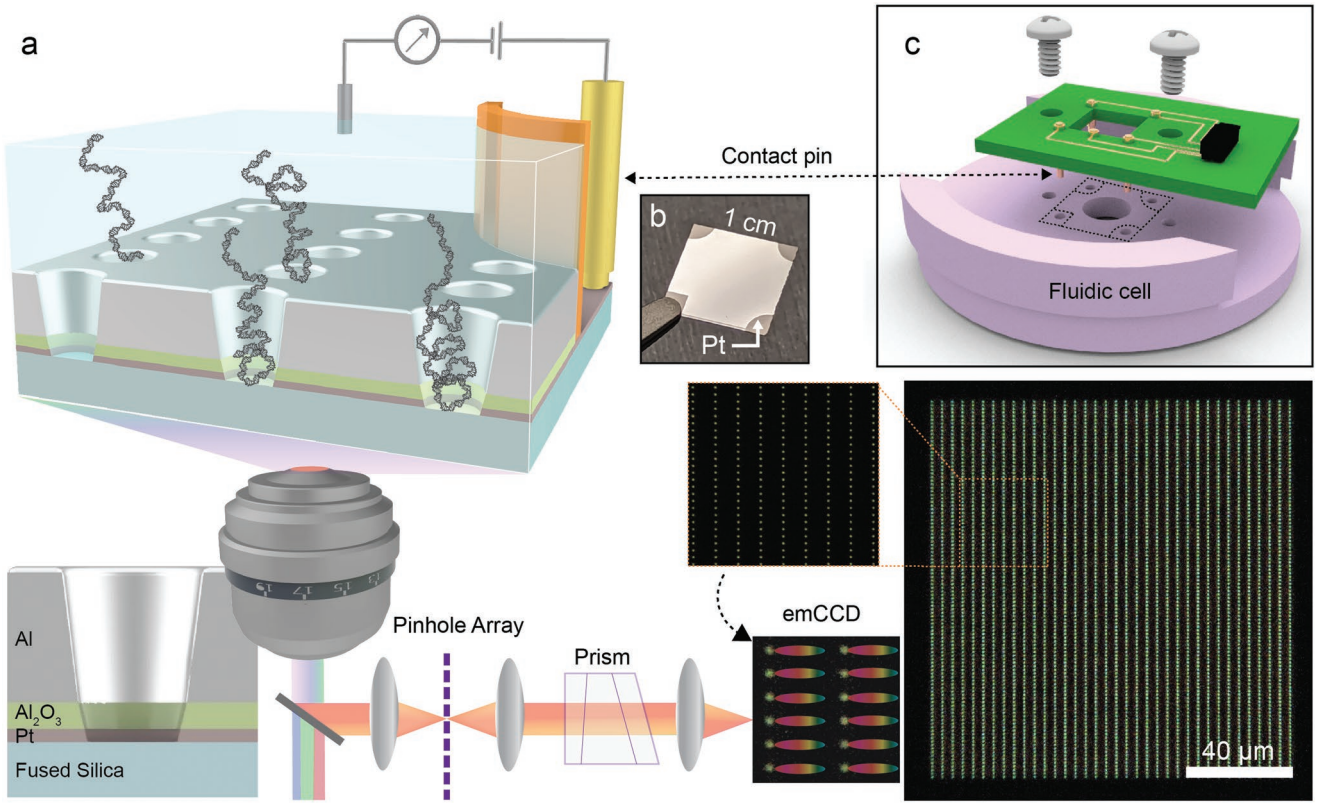

Figure 1. Electro-optical ZMWs (eZMWs) for DNA capture and sequencing. a) Scheme of an eZMW array placed on a fluorescence microscope coupled with a confocal pinhole array for background rejection and a prism which disperses emission spectra of four different dyes of labeled nucleotides to different angles on an electron-multiplying CCD (emCCD). Each eZMW is composed of Pt, Al, and Al_2O_3 layers, as seen in cross-section view shown in bottom left image. The bottom right microscopy image depicts a 36 × 106 array of eZMWs with a 4 µm × 1.33 µm pitch, the extra space between the waveguide columns designed for emission spectrum detection (a subset of the array is shown above to the left). b) Photograph of a 1 × 1 cm eZMW chip with exposed Pt layer at the chip corners to facilitate electrode contact. Each chip has four such eZMW arrays to allow four independent experiments. c) Exploded view of the fluidic cell integrated with a printed circuit board (PCB) for establishing electric contacts with the on-chip platinum layer through the four spring-loaded pogo pins.

to NZMWs and PZMWs, reduced background optical noise, and highly efficient length-independent DNA loading. We first model the electric field profile of eZMWs in optical wavelengths, confirming that the zero-mode effect occurs in these devices. Second, we study the electrochemical properties of the eZMW electrodes to confirm that a DC current can be generated upon voltage application. Third, we utilize voltage to characterize the capture of different-length DNA molecules into eZMWs. Finally, we perform SMRT sequencing to identify sequences from an equal concentration (picomolar level) mixture of a long and a short template based on data from a few-minute recording of real-time sequencing.

A schematic illustration of an eZMW-based device is shown in **Figure 1**a. The eZMW device is a fused silica chip that contains multiple 36 × 106 arrays of wells, each well comprising an aluminum cladding layer (top) that serves to generate a zero-mode light confinement effect. Underneath the Al layer, there is a thin dielectric alumina (Al_2O_3) layer that serves as an insulating layer, and below it is a thin (<10 nm) Pt-disk electrode which serves as a working electrode for application of electric fields within the waveguide. Upon voltage application between the platinum disk and another current-carrying platinum wire placed in the flowcell chamber that contains electrolyte and biomolecules, a strong localized electric field is created from local Faradaic reactions in the buffer within the eZMW. This localized field allows for efficient electrokinetic capture of DNA/RNA molecules that diffuse to the proximity of the well (cartoon in Figure 1a shows loaded DNA fragments). The eZMW device is placed atop a custom fluorescence microscope that allows three-wavelength excitation and broadband emission detection, and multicolor detection is achieved by transmitting the emission image through a prism[10] that provides the angular dispersion required for detection of all four phospholinked fluorescent nucleotides[3a] using an electron-multiplying charge-coupled device (emCCD) camera.

A photograph of an eZMW chip is shown in Figure 1b. To facilitate electrical contact with the Pt disk electrode embedded underneath the waveguides, we etched the Al and Al_2O_3 layers at the four corners of the chip using a standard photolithography process. The exposed Pt is then isolated from the rest of the chip using SU-8 to prevent liquid contact (Figure 1a, illustrated as an orange barrier layer). In a typical experiment, the eZMW chip is mounted on the bottom side of a poly(ether ether ketone) (PEEK) fluidic cell (see Figure 1c) that contains our fused silica chip on its bottom. The cell also has a printed circuit board (PCB) interface onto which conductive spring-loaded

pogo pins have been soldered to allow electrical connection to a patch clamp amplifier (Axopatch 200B) for voltage application between the on-chip Pt layer and the Pt wire electrode present in the sample chamber.

2. Optical Characterization of eZMWs

In SMRT sequencing, DNA replication by a DNA polymerase is tracked in real-time using ZMWs, which are used to achieve single-molecule fluorescence sensitivity within a small observation volume (zeptoliters) in the presence of a buffer solution that contains a relatively high concentration (0.01×10^{-6} to 1×10^{-6} M) of phospholinked fluorescent deoxyribonucleotides (dNTPs).[3a,11] To guide the design of our eZMWs, we have performed 3D finite-element simulations of electric field intensity inside 100 nm diameter eZMW with different thicknesses of Al_2O_3 spacer between the 100 nm aluminum and 8 nm platinum layers of the device in the overall excitation/emission range in our experiments (500–800 nm) (see Section S1 in the Supporting Information for more details). In **Figure 2**a, we compare intensity decay profile for an eZMW with the optimized thickness of Al_2O_3 spacer (40 nm) and the standard aluminum-based waveguide (AlZMW) at green (532 nm) and red (640 nm) wavelengths. According to the simulation results, the electric field (light) intensity profile along the *z*-axis within the eZMW shows ZMW-typical attenuation for both wavelengths, and while the characteristic decay length is not as small as for AlZMWs, eZMWs allow high-quality single-molecule sequencing measurements, as we later show. In Figure 2b, we show field enhancement comparison of eZMWs with different Al_2O_3 thicknesses (*t*) and AlZMW at point A which is chosen to represent a likely position of a DNA polymerase that is surface-tethered (i.e., 10 nm above the SiO_2 to account for the organic passivation layer thickness). The simulation results indicate that the field at point A is higher in the layered eZMW structure as compared to the case of a bare aluminum ZMW (AlZMW).[11b] The field at point A is enhanced for increasing Al_2O_3 thickness from 10 to 80 nm, with greater changes in the enhanced field in red (640 nm) wavelengths than for green (532 nm) wavelengths (see Figure S2a in the Supporting Information). Furthermore, the field is smaller at 640 nm (red), but depends much more on the Al_2O_3 thickness than for the 532 nm wavelength (green). However, while increasing the thickness of the Al_2O_3 layer to 80 nm results in larger observation volume in both red and green lasers (see Figure S2b in the Supporting Information), the overall ZMW volume increases, and therefore the amount of background from diffusing phospholinked fluorescent nucleotides is larger. Considering this trade-off between increasing ZMW volumes and electrical field enhancement, we chose a thickness of 40 nm for our Al_2O_3 insulator layer. For this thickness, we present a false color map of the electric field

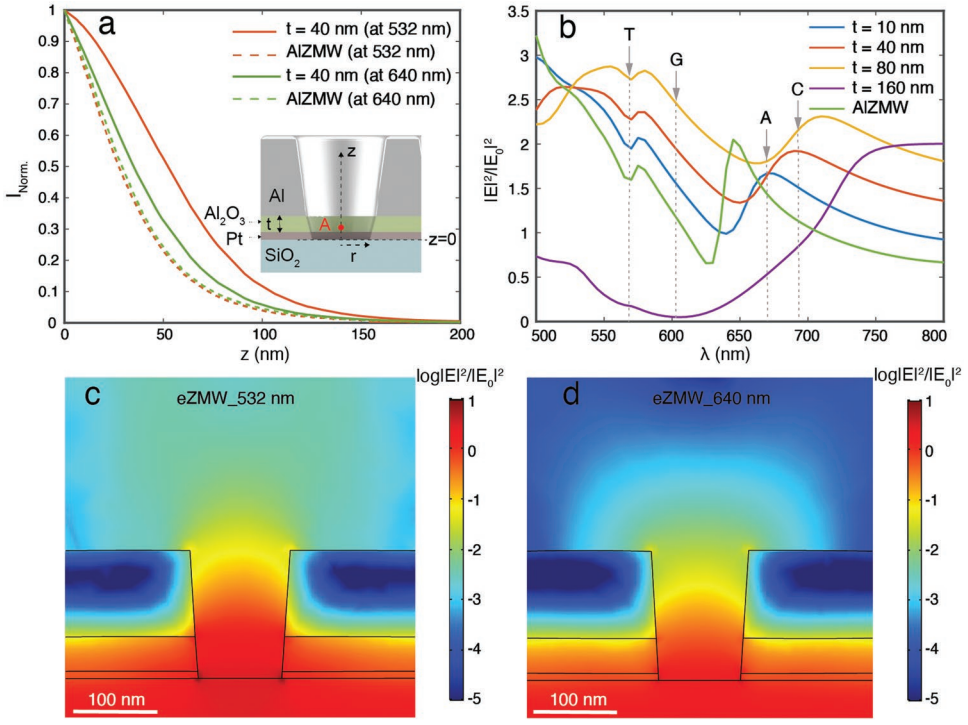

Figure 2. Optical performance of the eZMW. 3D finite-element simulations of a 100 nm bottom diameter eZMW with 100 nm-thick Al, 8 nm-thick Pt, and Al_2O_3 thickness *t*. a) Comparison of intensity decay profile along the *z*-axis for an eZMW with 40 nm-thick Al_2O_3 and an AlZMW at 532 and 640 nm (AlZMW represents a single layer 100 nm-thick Al ZMW for comparison). The inset shows the *z*-axis and other parameters used in the simulation on a cross-section view of an eZMW. b) Field enhancement comparison of eZMWs with different Al_2O_3 thicknesses (*t*) and AlZMW at point A ($z = 10$ nm, $r = 0$) (approximate position of a DNA polymerase) for 500–800 nm spectrum (the fluorescence emission wavelength windows (as marked by T, G, A, C) of the labeled nucleotides) ($E_0^2 = 1\ V^2\ m^{-2}$). c,d) 3D finite-element simulation of the intensity distribution (log scale) for the eZMW with 40 nm of Al_2O_3 at 532 nm (c) and 640 nm (d).

in space within the eZMW for 532 nm (Figure 2c) and 640 nm (Figure 2d), which shows that light is attenuated greatly within the guide for both lasers, similarly to results found for Al-based ZMWs and dual-ring electrode ZMWs,[11b,12] and decays by 0.5 orders of magnitude within ≈50 nm *z*-height for 640 nm light in eZMWs of radii that range from 50 to 70 nm (see Figure S2c in the Supporting Information).

3. eZMW Structural Characterization

eZMWs are fabricated on UV-grade 170 µm-thick fused silica wafers via standard electron-beam lithography, layer-by-layer deposition, and lift-off methods. Briefly, a negative tone e-beam resist is spun-coated on a wafer, followed by scanning a focused beam of electrons to make patterns corresponding to the eZMW array. This results in nanopillars remaining on the wafer, which is then deposited with successive layers of Ti, Pt, Al_2O_3, and Al using an e-beam evaporator. Next, the resist pillars along with the metal caps are dissolved leaving behind nanoapertures, the imprint of the pillars (see Figure S3 in the Supporting Information). Then, photolithography is performed on the aluminum side of the wafer to expose only the four corners that will be etched to provide access to the Pt layer, followed by etching of the Al and Al_2O_3 layers. Finally, the wafers with exposed Pt areas are diced into individual 1 cm × 1 cm chips (see Figure 1b).

Figure 3a shows a scanning electron microscopy (SEM) image of a 3 × 9 subset of a 36 × 106 eZMW array (Figure 1a, bottom right image) in which ZMWs are spaced 1.33 µm (short axis) and 4.0 µm (long axis). The inset of Figure 3a shows the top-view SEM image of an eZMW. The bright outline around each eZMW is an artifact that stems from its slanted shape that forms due to a shadowing effect from the pillars during the metal deposition process.[13] This is confirmed by the image in Figure 3b, which shows a cross-sectional view of the eZMW generated by focused ion beam (FIB) milling a thin lamella and transferring it to a transmission electron microscopy (TEM) grid (see the Experimental Section). Figure 3c shows a further close-up view of the TEM cross-sectional image in Figure 3b, in which the layers are seen more clearly, using both TEM and SEM imaging, we have determined that the top and base diameters are 200 ± 10 and 100 ± 10 nm, respectively (see Figure S4 in the Supporting Information). To confirm the elemental composition of each layer in the eZMW, in Figure 3d, we present a high-resolution energy-dispersive X-ray spectroscopy (EDS) map on the sample shown in Figure 3b,c. The false colors in the map are attributed to the different elements, as shown in the legend.

4. Electrical Performance of eZMWs

Figure 4a,b depicts current–voltage (*I–V*) curves measured on an array of eZMWs in 10×10^{-3} M KCl (1× Tris–ethylenediaminetetraacetic acid (EDTA), pH 8.0) and sequencing buffer under different voltage biases, respectively. The recorded *I–V* curves for 10×10^{-3} M KCl buffer, which represent 5 successive voltage sweep cycles, exhibit a highly symmetrical hysteresis behavior caused by capacitance at the electrode/solution interface. By contrast, this hysteresis behavior is weaker and the current magnitude is higher in the sequencing buffer, due to a higher extent of Faradaic reactions produced by redox-active agent, nitrobenzoic acid (NBA) in the sequencing buffer (see Figure S5 in the Supporting Information). The insets in Figure 4a,b show typical current–time (*I–t*) traces of an eZMW in 10×10^{-3} M KCl (1× Tris–EDTA, pH 8.0) and sequencing buffer for different voltages, respectively. In contrast to the case of pure KCl electrolyte, the sequencing buffer, which contains a redox-active species NBA, produces a steady current level that hints on Faradaic processes at the electrodes. We made sure that the current produced is not due to the aluminum corrosion by inspecting eZMW arrays after electrical measurements (see Figure S6 in the Supporting Information). To further investigate the signal amplification by redox recycling, we studied the electrochemical performance of eZMWs in 5×10^{-3} M $K_3Fe(CN)_6$ and 5×10^{-3} M $K_4Fe(CN)_6$ solution with 10×10^{-3} M aqueous KCl supporting electrolyte (see Figure S7 in the Supporting Information). A steady state current is observed which attributes to redox cycling reaction of reversible electroactive species of $Fe(CN)_6^{4-}$ and $Fe(CN)_6^{3-}$ in the diffusion-controlled electrochemical loop. In the absence of a Faradaic reaction, capacitance that results from the ion double layer at the electrode/electrolyte interface dominates the current behavior. To further delineate Faradaic versus

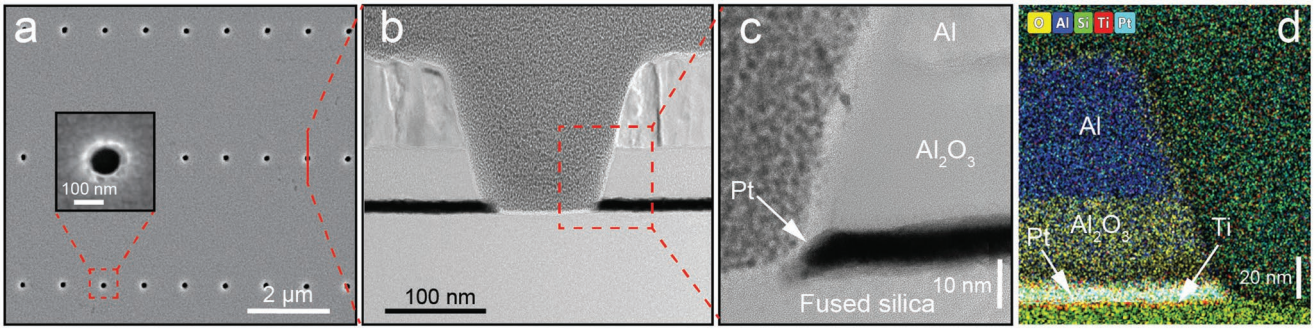

Figure 3. Structural characterization of eZMWs. a) SEM image of a 3 × 9 eZMW array. A close-up view of a single eZMW is shown in the inset. b) TEM image cross-sectional view of an eZMW shows the tapered waveguide structure (see text). c) Close-up view of the eZMW shown in (b). d) False-color map from scanning/transmission electron microscopy (S/TEM) with energy-dispersive X-ray spectroscopy (EDS) which maps the eZMW shown in (b,c).

non-Faradaic current sources in the signal, we have measured *I–V* curves at different voltage scan rates (see Figure S8 in the Supporting Information). We find that the anodic and cathodic peak currents are linearly dependent on the square root of the scan rate in the sequencing buffer for all voltages ($R^2 > 0.99$ for all fits). This result indicates that a diffusion-controlled process exists on the Pt electrodes, and furthermore, its contribution is greater than the capacitive current according to the Randles–Sevcik equation.[14]

5. Loading Efficiency in eZMWs

Since eZMWs were designed to overcome the high input DNA requirements and length bias of diffusion-based loading, we investigated here voltage-driven DNA loading into eZMWs by fluorescently labeling various-length fragments of double-stranded DNA (dsDNA) with the intercalating dye DiYO (AAT Bioquest, Sunnyvale, CA) and continuously monitoring fluorescence under blue laser (488 nm) excitation. **Figure 5**a displays integrated fluorescence snapshots up to indicated loading times of a 1×10^{-9} M 500 bp DNA solution at +100 mV applied voltage. Clearly, the number of active ZMWs rises over time, which points to a time-stable capture of DNA molecules inside the eZMWs (note: there is no chemistry to tether the molecules to the surface in this experiment). In Figure 5b–d, we present loading percent as a function of time based on statistics from three independent devices as a function of DNA length, concentration, and voltage, respectively. Although electrokinetic loading is expected to eliminate all length bias, we observe an approximately threefold increased loading efficiency for 500 bp DNA, as compared with 48.5 kbp (Figure 5b), a relatively insignificant bias considering the order of magnitude larger radius of gyration of 48.5 kbp DNA (≈500 nm) as compared to 500 bp (≈50 nm). As expected, DNA loading is concentration-dependent, with initial loading rates approximately proportional to the concentrations, as seen in Figure 5c. Finally, increasing the voltage has a drastic effect on loading rates, as presented in Figure 5d, which shows loading trajectories for 10×10^{-12} M 500 bp DNA at voltages in the range of –100 to 500 mV (also see Movie S1 in the Supporting Information). These results show that negative voltage repels DNA from the eZMW, more effectively than in the case of a passive (no voltage) eZMW, while a high positive voltage greatly promotes DNA capture. Upon application of a voltage bias, a localized field is created (within hundreds of nanometers from the ZMW "mouth"), sufficient to capture/trap DNA molecules present in the vicinity of the ZMWs.[8,9] For the data in Figure 5b–d, we have used the simplified 1:1 binding kinetics equation $F(t) = C \times (1 - e^{-kt})$ in which C is the normalized concentration term and k is the binding constant between the DNA and the eZMW, neglecting off rates since our data are time integrated (no unbinding is taken into account).[15]

6. Single-Molecule Characterization of eZMWs

The high loading efficiency of DNA molecules into eZMWs, as well as the low observation volume of the new layered structure, paves the way for low-input DNA sequencing studies. **Figure 6**a presents a cartoon of a single eZMW and the electrical configuration of the fluidic cell. To prevent nonspecific adsorption of molecules to the Al/Al_2O_3 surface, the metal aluminum cladding surface was passivated through the use of poly(vinylphosphonic acid) (PVPA) chemistry,[16] and to allow binding of polymerase to the eZMW base, the bottom surface of the eZMWs is coated with interspersed biotin groups (black triangles) and an antifouling poly(ethylene glycol) layer (not shown). Voltage application between the Pt layer within the eZMW and a Pt wire in solution creates an electric field (dashed red arrows represent the electric field lines) that draws a DNA SMRTbell (see Figure S9a in the Supporting Information for SMRTbell structure) complexed with a polymerase–streptavidin fusion protein (Pol–Stv) into the eZMW. Although

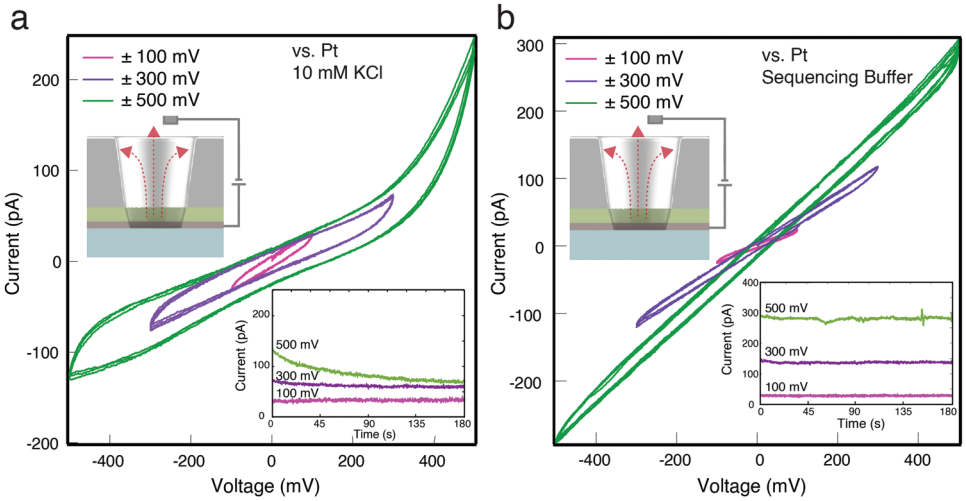

Figure 4. eZMW electrical performance. a) *I–V* characteristics of the eZMW chip versus platinum electrode for different voltages during 5 voltage-sweep cycles at scan rate of 10 mV s^{-1} in 10×10^{-3} M KCl. b) *I–V* characteristics of the eZMW chip versus platinum electrode for different voltages during 5 voltage-sweep cycles at scan rate of 10 mV s^{-1} in sequencing buffer. In all cases, the voltage sweeps are reproducible and overlapping, indicating electrochemical stability of the device. Insets: current versus time curve of the eZMW chips for different applied voltages.

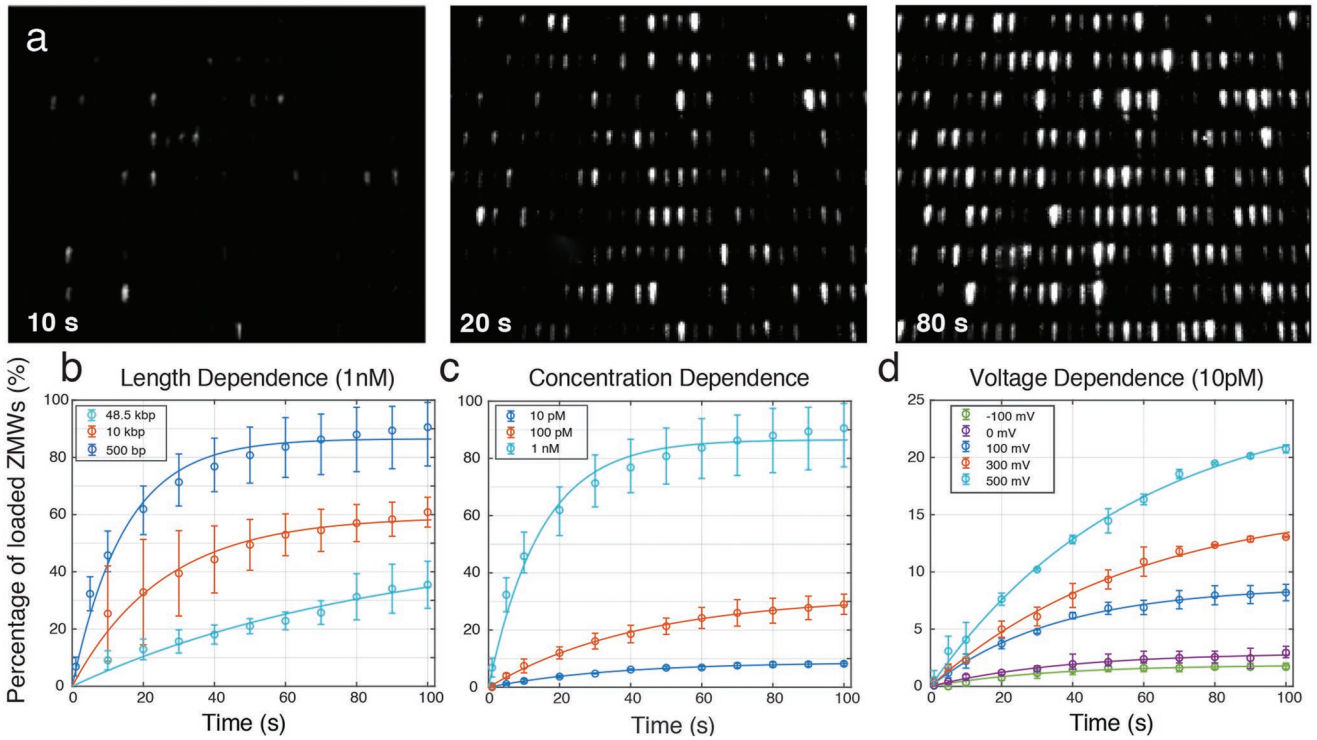

Figure 5. Loading efficiency in eZMWs. a) Frame-integrated images of loading 500 bp DiYO-labeled DNA after 10, 20, and 80 s of 100 mV voltage application (DNA concentration: 1×10^{-9} M). b) Percentage of loaded ZMWs in 100 s for 500 bp, 10 kbp, and 48.5 kbp DiYO-labeled DNAs at a total concentration of 1×10^{-9} M in the presence of 100 mV voltage bias. c) Percentage of loaded ZMWs in 100 s for 10×10^{-12}, 100×10^{-12}, and 1×10^{-9} M of 500 bp DNA in the presence of 100 mV voltage bias. d) Percentage of loaded ZMWs in 100 s for 10×10^{-12} M of 500 bp DNA in the presence of −100, 0, 100, 300, and 500 mV voltage bias (see Movie S1 in the Supporting Information). The error bars represent one standard deviation of the mean from three different experiments performed using different devices. The curves for each dataset are best fits using the simple 1:1 binding model $F(t) = C \times (1 - e^{-kt})$, where C is the normalized concentration and k is the binding constant (see Table S1 in the Supporting Information for the fit coefficients).

a single eZMW is shown in the cartoon, voltage loading occurs on a whole array of eZMWs, as shown in Figure 5. Here, we loaded a mixture of 260 bp and 20 kbp SMRTbells (see Figure S9b in the Supporting Information for rolling circle amplification gel confirming SMRTbell structure) complexed with Pol–Stv into eZMWs from a 67×10^{-12} M bulk concentration (260 bp: 11 pg μL^{-1}, 20 kbp: 870 pg μL^{-1}) using a 60 s 400 mV voltage pulse.

Once loaded, the buffer solution is supplemented with a Mg^{2+}-containing buffer, which initiates polymerase activity and DNA sequencing is achieved by monitoring the fluorescence pulses that occur during incorporation of phospholinked dNTPs. To achieve DNA sequencing with sufficient spectral resolution, emission from each eZMW in the array is routed through a confocal pinhole to reject undesired background,[10] as well as a dispersive prism for 4-color discrimination of the labeled nucleotides (see Figure S10a in the Supporting Information). In this configuration, each fluorescent dNTP appears in a different vertical position on the emCCD image (see Figure S10b in the Supporting Information).[10] The voltage loading pulse used in this experiment resulted in 38% of the eZMWs being fluorescence-active, which is in good accordance with the loading fraction expected for 260 bp (54%) and 20 000 bp (24%) SMRTbells based on the capture experiments in Figure 5. In Figure 6b, we show individual frames focused on a single eZMW which were selected from a SMRT sequencing recording at 83.7 frames s^{-1}. As seen in the successive frames, nucleotide incorporation produces pulses in either of two zones, Z1 and Z2, that correspond to dyes excited with green and red excitation, respectively. In one of the frames, boxed in red, a transition from A to G to A occurred too fast, such that the signal for G appeared concurrently with the signal for A. This type of event and other similar confounding signals necessitate visual inspection after a preliminary software-based basecalling algorithm was applied to the dataset (see Figure S11 in the Supporting Information for details of the analysis). Underneath the selected frames, we show a typical intensity versus time trace for a 3.6 s recording that produced a 22/23 nucleotide alignment with one of the DNA template reference sequences (260 bp SMRTbell). The colors of the peaks in the intensity plot represent the assigned base in the DNA sequence (also indicated by a letter), based on the position of the burst and its intensity. The gray trace overlaid on the "signal" trace represents the intensity of pixels in the zone for which no dye emission was observed. In Figure 6c, an image that results from integrating the frames acquired from a 2 min recording of an eZMW array during the SMRT-sequencing experiment is shown. Applying the basecalling algorithm to the active wells, we were able to align very short reads (few seconds) to the SMRTbell templates with an average accuracy of 96.35 ± 3.05% for both fragments, as well as min–max *E*-value (expected value) of 6×10^{-14} to 8×10^{-4} for the correct template and 0.31–11 for the wrong template (see Figure 6c, Figure S11, and Table S2

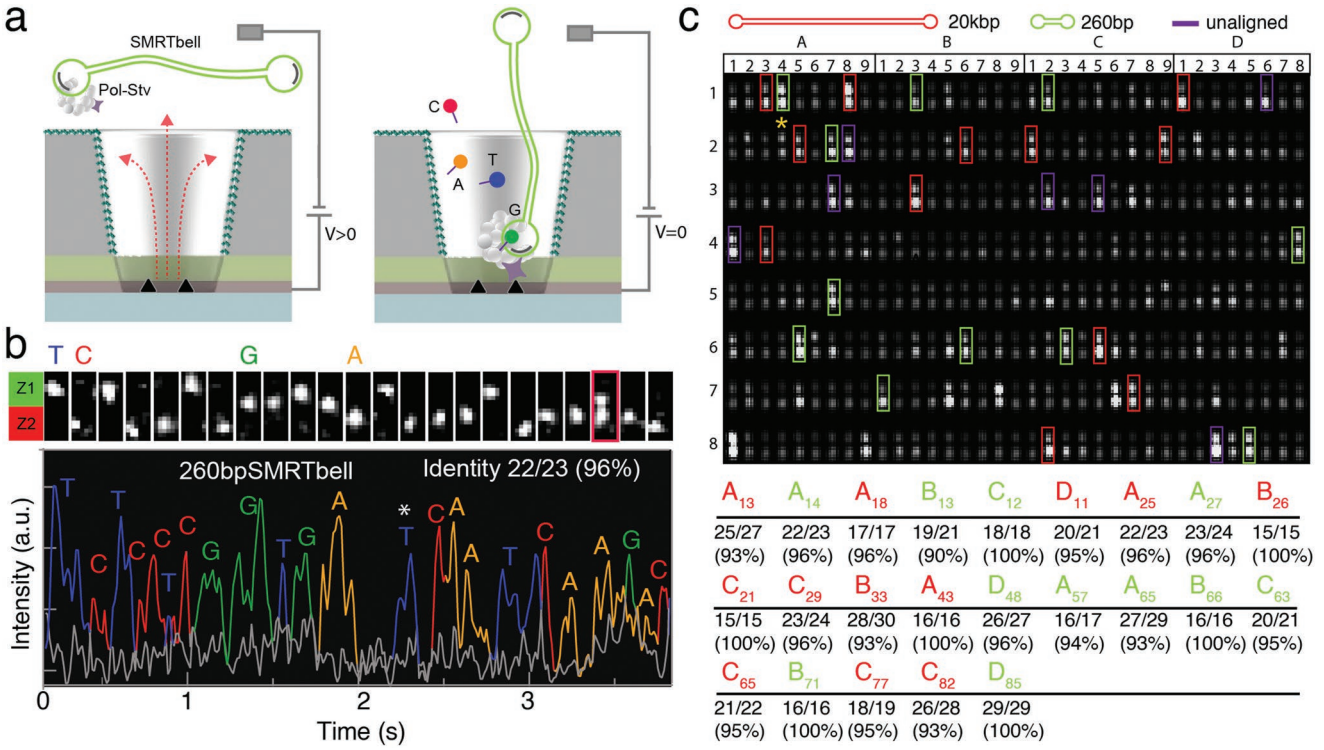

Figure 6. Rapid SMRT-Seq identification of DNA fragments using eZMWs. a) Left: schematic of a primed DNA SMRTbell (green) bound to a DNA polymerase/streptavidin fusion protein (Pol–Stv) captured by an electric field (dashed red line) into an eZMW. Once bound, the streptavidin binds to a surface biotin group present on the base of the eZMW (black triangle). Right: after loading, polymerase activity is initiated upon Mg^{2+} addition, and fluorescence from the phospholinked fluorescent dNTP reports on DNA sequence. b) Top: frames picked from a movie recording focused on a single eZMW, where successive nucleotide incorporation is seen in two zones (Z1 for green dyes and Z2 for red dyes). Bottom: intensity versus time trace for a 3.6 s recording that produced a 22/23 nucleotide alignment with a reference. The intensity plot is false colored to represent the assigned base in the DNA sequence, indicated by a letter, based on the position of the peak along the vertical axis of the frames from the recording (overlaid gray trace represents intensity of pixels in the inactive zone). c) Top: integrated stack from the first 120 s of recording an eZMW array during SMRT sequencing a mixture of loaded 260 bp and 20 kbp SMRTbells (SMRTbell concentrations were 67×10^{-12} M, loaded at 400 mV for 60 s). Green and red boxes represent eZMWs that aligned to 260 bp and 20 kbp sequences, respectively. The eZMW marked with a yellow asterisk (A_{14}) contained the 260 bp SMRTbell shown in (b). Bottom: table of accuracy and read length for various eZMWs in the array, all obtained from a few-minute recording (see Movie S2 in the Supporting Information). The eZMW that corresponds to each read is designated by its position in the matrix.

in the Supporting Information). Apart from the 23 wells that showed clear 4 color sequencing in the first few minutes, 7 of the wells did not align with any of the templates, and the remaining 76 active wells had either multiple molecules in a well, a low signal-to-noise ratio, frequent polymerase stalling, or sporadic fluorescence signals, indicative of low polymerase activity.

7. Conclusions

We have demonstrated here a new device for electrical capture of DNA into ZMWs fabricated on a solid fused silica substrate. These devices enable the two important features required for efficient SMRT sequencing from low inputs: the light confining impact of zero-mode waveguides, and the ability to produce electrical fields in order to capture DNA fragments. We have shown that capture of DNA molecules is greatly enhanced by applying voltage to the Pt electrode at the base of the eZMWs, and further, that short and long fragments can be captured with high efficiency and relatively low length bias (100-fold increase in DNA length results in only a 1/2 decrease in capture efficiency). Using these devices, we have captured from an equimolar mixture of short (260 bp) and long (20 kbp) DNA fragments (picomolar level) and demonstrated rapid sequence readout from these fragments in an eZMW array. Very fast (minute long) movies produced sequence readouts that mapped to the references, enabling rapid identification of these fragments. These eZMW devices open new avenues in low-input DNA sequencing, particularly epigenetics studies where the native DNA extracted from a sample needs to be analyzed without any amplification steps.

8. Experimental Section

Sample Molecule Preparation: DiYO-labeled DNA was prepared from 500 bp, 10 kbp, and λ-DNA (Thermo Fisher Scientific) and DiYO-1 intercalating dye (AAT Bioquest, Sunnyvale, CA, USA) in a 10×10^{-3} M KCl buffer, pH 8. A 10:1 base pair-to-dye molar ratio of dsDNA molecules was incubated with DiYO-1 dye for 20 min at 50 °C. The 260 bp/20 kbp SMRTbell template (Pacific Biosciences) was annealed to the primer with 20× stoichiometric ratio in 10× primer buffer. The primer-bound 260 bp/20 kbp SMRTbell template (Pacific Biosciences) was incubated

with DNA polymerase (Pacific Biosciences P6) with 10× stoichiometric ratio at 30 °C for 30 min (proprietary buffer solutions). Samples were then put in 50% glycerol with dithiothreitol and placed at −20 °C for storage prior to use.

Surface Treatment: Chips were cleaned by acetone and isopropanol, dried with a nitrogen stream, and subjected to an oxygen plasma (Technics) at 50 W for 60 s. To passivate the aluminum surface, the chips were immersed in 90 °C preheated 0.5% aqueous solution of PVPA (Pacific Biosciences) for 2 min at 90 °C.[16] They were rinsed thoroughly with deionized (DI) water, dried with a nitrogen stream, and annealed on a hot plate at 85 °C for 10 min. After annealing, eZMW chips were immersed in 0.5 mg mL^{-1} biotin–poly(ethylene glycol)–silane dissolved in 200 proof ethanol for 2 h at room temperature to functionalize the eZMW bottom surface for specific attachment of the polymerase carrying an N-terminal biotin tag.

Data Acquisition and Analysis: Top-view SEM image of eZMWs was acquired using a FEI Scios Dualbeam system with field-emission scanning election microscope at 5 kV. FIB on a FEI Scios Dualbeam system was used to create very precise cross-sections of eZMWs for scanning/transmission electron microscopy (S/TEM) imaging. A protective Pt layer was deposited on top of ZMWs during FIB process. Probe-corrected FEI Titan Themis 300 S/TEM with ChemiSTEM technology was used for S/TEM and EDS characterizations. TEM images were carried out at 300 kV. EDS spectrum and mapping analysis were performed at 300 kV using a Super-X EDS system.

The eZMW chips were assembled from the bottom side of a prototype PEEK fluidic cell. The chamber of the flow cell was filled with 10×10^{-3} M KCl, 1× Tris–EDTA, pH 8.0 electrolyte and a Pt wire electrode (0.3 mm thick) was inserted to it and connected to an Axon 200B patch-clamp amplifier to measure the ionic current. Voltage was applied through the Pt wire and Pt electrode layer embedded into the ZMWs. To make a reliable electrical connection with the Pt layer, four spring-loaded connectors (pogo pins) were soldered to a custom-designed PCB which was clamped to the fluidic cell. The pogo pins with gold over nickel shell and inner spring plating were positioned at the four corners of the chip to contact the exposed Pt layer of the chip.

The cell was mounted in a Faraday cage on the stage of an Olympus IX81 inverted microscope with a 60×, 1.49 numerical aperture (NA) oil immersion objective. The bottom side of the chip was illuminated with a Coherent Cube 640 nm laser, Coherent Compass 315M-100 532 nm laser (for SMRT sequencing experiments), and a Coherent Sapphire 488 nm laser (for DNA capture experiments). Electrical data were recorded using custom-made LabVIEW software (National Instruments, Woburn, MA, USA). Images were taken with an iXon Ultra 897 emCCD camera, recorded with HCImage Live software (Hamamatsu, Sewickley, PA, USA), and analyzed with ImageJ.

Chip Preparation: A standard photolithography process was used to make alignment features for dicing and areas for the electrode connection. First wafers were coated with S1813 photoresist and patterned using KarlSuss MA6/BA6 mask aligner. After exposure, wafers were immersed in MF-319 developer for 3 min to develop the photoresist, as well as to etch the aluminum and alumina at the exposed areas. The wafers were then diced into 10 × 10 mm square chips by aligning the dicing tool with the larger features patterned on the chips during the photolithography step.

Supporting Information

Supporting Information is available from the Wiley Online Library or from the author.

Acknowledgements

The authors acknowledge Dr. Mohammad Amin Alibakhshi for eZMW device design and fabrication, DNA capture experiments and data analysis, and guidance with the project. The authors acknowledge Dr. Jonas Korlach (Pacific Biosciences) for advice and critical feedback on the paper. The authors acknowledge Dr. Yu-Chih Tsai (Pacific Biosciences) for aid in sample preparation; Dr. Jason Sutin for advice on setting up the optical setup; Dr. Jacob Rosenstein for guidance on the PCB design; Ali Fallahi and Mohammad Nabizadehmashhadtoroghi for their assistance with the basecalling software. SEM and TEM images were acquired at the Kostas Advanced Nano-Characterization Facility (KANCF) in Burlington, and some of the device fabrication at Northeastern's George J. Kostas Nanoscale Technology and Manufacturing Research Center. This work was performed in part at the Cornell Nanoscale Facility (CNF), a member of the National Nanotechnology Coordinated Infrastructure (NNCI), which is supported by the National Science Foundation (Grant No. ECCS-1542081). This work was supported by the NIH/National Human Genome Research Institute Grant Nos. HG009186 and HG011087. Y.L. acknowledges the support of the National Science Foundation under Grant Number CBET-1931777.

Conflict of Interest

The authors declare no conflict of interest.

Data Availability Statement

The data that support the findings of this study are openly available in Figshare at https://figshare.com/s/83631a15d4ecf961d205.

Keywords

rapid DNA identification, single-molecule sequencing, zero-mode waveguides

Received: October 21, 2021
Revised: December 18, 2021
Published online:

[1] a) W. R. Jeck, J. Lee, H. Robinson, L. P. Le, A. J. Iafrate, V. Nardi, *J. Mol. Diagn.* **2019**, *21*, 58; b) A. L. Greninger, S. N. Naccache, S. Federman, G. Yu, P. Mbala, V. Bres, D. Stryke, J. Bouquet, S. Somasekar, J. M. Linnen, R. Dodd, P. Mulembakani, B. S. Schneider, J.-J. Muyembe-Tamfum, S. L. Stramer, C. Y. Chiu, *Genome Med.* **2015**, *7*, 99; c) S. Datta, R. Budhauliya, B. Das, S. Chatterjee, V. V. Vanlalhmuaka, *World J. Virol.* **2015**, *4*, 265; d) A. A. Nkili-Meyong, L. Bigarré, I. Labouba, T. Vallaeys, J. C. Avarre, N. Berthet, *Intervirology* **2016**, *59*, 285.

[2] a) H. Krehenwinkel, M. Wolf, J. Y. Lim, A. J. Rominger, W. B. Simison, R. G. Gillespie, *Sci. Rep.* **2017**, *7*, 17668; b) J. Dabney, M. Meyer, *BioTechniques* **2012**, *52*, 87; c) H. Shi, Y. Zhou, E. Jia, M. Pan, Y. Bai, Q. Ge, *BioMed Res. Int.* **2021**, *2021*, 6647597; d) F. Syed, H. Grunenwald, N. Caruccio, *Nat. Methods* **2009**, *6*, https://doi.org/10.1038/nmeth.f.269; e) S. R. Head, H. K. Komori, S. A. LaMere, T. Whisenant, F. Van Nieuwerburgh, D. R. Salomon, P. Ordoukhanian, *BioTechniques* **2014**, *56*, 61.

[3] a) J. Eid, A. Fehr, J. Gray, K. Luong, J. Lyle, G. Otto, P. Peluso, D. Rank, P. Baybayan, B. Bettman, A. Bibillo, K. Bjornson, B. Chaudhuri, F. Christians, R. Cicero, S. Clark, R. Dalal, A. Dewinter, J. Dixon, M. Foquet, A. Gaertner, P. Hardenbol, C. Heiner, K. Hester, D. Holden, G. Kearns, X. Kong, R. Kuse, Y. Lacroix, S. Lin, et al., *Science* **2009**, *323*, 133; b) E. E. Schadt, S. Turner, A. Kasarskis, *Hum. Mol. Genet.* **2010**, *19*, R227; c) M. Jain,

H. E. Olsen, B. Paten, M. Akeson, *Genome Biol.* **2016**, *17*, 239; d) J. Clarke, H. C. Wu, L. Jayasinghe, A. Patel, S. Reid, H. Bayley, *Nat. Nanotechnol.* **2009**, *4*, 265.

[4] a) E. W. Loomis, J. S. Eid, P. Peluso, J. Yin, L. Hickey, D. Rank, S. McCalmon, R. J. Hagerman, F. Tassone, P. J. Hagerman, *Genome Res.* **2013**, *23*, 121; b) S. Ardui, A. Ameur, J. R. Vermeesch, M. S. Hestand, *Nucleic Acids Res.* **2018**, *46*, 2159; c) D. Pedone, M. Langecker, G. Abstreiter, U. Rant, *Nano Lett.* **2011**, *11*, 1561; d) X. Liu, M. Mihovilovic Skanata, D. Stein, *Nat. Commun.* **2015**, *6*, 6222; e) J. Han, S. W. Turner, H. G. Craighead, *Phys. Rev. Lett.* **1999**, *83*, 1688.

[5] Pacific Biosciences, Procedure and Checklist: 20 kb Template Preparation Using BluePippin Size-Selection System (**2015**), https://www.pacb.com/wp-content/uploads/2015/09/Procedure-Checklist-20-kb-Template-Preparation-Using-BluePippin-Size-Selection.pdf (accessed: January 2022).

[6] Pacific Biosciences, Procedure & Checklist: 10 kb Template Preparation and Sequencing (with Low-Input DNA) (**2014**), https://www.pacb.com/wp-content/uploads/2015/09/Procedure-Checklist-10-kb-Template-Preparation-and-Sequencing-with-Low-Input-DNA.pdf (accessed: January 2022).

[7] a) C. Raley, D. Munroe, K. Jones, Y.-C. Tsai, Y. Guo, B. Tran, S. Gowda, J. L. Troyer, D. R. Soppet, C. Stewart, R. Stephens, J. Chen, T. Skelly, C. Heiner, J. Korlach, D. Nissley, *bioRxiv* **2014**, https://doi.org/10.1101/003566; b) P. Coupland, T. Chandra, M. Quail, W. Reik, H. Swerdlow, *BioTechniques* **2012**, *53*, 365.

[8] a) J. Larkin, M. Foquet, S. W. Turner, J. Korlach, M. Wanunu, *Nano Lett.* **2014**, *14*, 6023; b) J. Larkin, R. Y. Henley, V. Jadhav, J. Korlach, M. Wanunu, *Nat. Nanotechnol.* **2017**, *12*, 1169.

[9] V. Jadhav, D. P. Hoogerheide, J. Korlach, M. Wanunu, *Nano Lett.* **2019**, *19*, 921.

[10] P. M. Lundquist, C. F. Zhong, P. Zhao, A. B. Tomaney, P. S. Peluso, J. Dixon, B. Bettman, Y. Lacroix, D. P. Kwo, E. McCullough, M. Maxham, K. Hester, P. McNitt, D. M. Grey, C. Henriquez, M. Foquet, S. W. Turner, D. Zaccarin, *Opt. Lett.* **2008**, *33*, 1026.

[11] a) I. D. Vilfan, Y.-C. Tsai, T. A. Clark, J. Wegener, Q. Dai, C. Yi, T. Pan, S. W. Turner, J. Korlach, *J. Nanobiotechnol.* **2013**, *11*, 8; b) M. J. Levene, J. Korlach, S. W. Turner, M. Foquet, H. G. Craighead, W. W. Webb, *Science* **2003**, *299*, 682.

[12] D. Han, G. M. Crouch, K. Fu, L. P. Zaino III, P. W. Bohn, *Chem. Sci.* **2017**, *8*, 5345.

[13] M. Foquet, K. T. Samiee, X. Kong, B. P. Chauduri, P. M. Lundquist, S. W. Turner, J. Freudenthal, D. B. Roitman, *J. Appl. Phys.* **2008**, *103*, 034301.

[14] N. Elgrishi, K. J. Rountree, B. D. McCarthy, E. S. Rountree, T. T. Eisenhart, J. L. Dempsey, *J. Chem. Educ.* **2018**, *95*, 197.

[15] T. Morton, D. Myszka, I. Chaiken, *Anal. Biochem.* **1995**, *227*, 176.

[16] J. Korlach, P. J. Marks, R. L. Cicero, J. J. Gray, D. L. Murphy, D. B. Roitman, T. T. Pham, G. A. Otto, M. Foquet, S. W. Turner, *Proc. Natl. Acad. Sci. USA* **2008**, *105*, 1176.